

Domain Adaptation Using Adversarial Learning for Autonomous Navigation

Jaeyoon Yoo^{*1} Yongjun Hong^{*1} YungKyun Noh¹ Sungroh Yoon¹

Abstract

Autonomous navigation has become an increasingly popular machine learning application. Recent advances in deep learning have also brought huge improvements to autonomous navigation. However, prior outdoor autonomous navigation methods depended on various expensive sensors or expensive and sometimes erroneously labeled real data. In this paper, we propose an autonomous navigation method that does not require expensive labeled real images and uses only a relatively inexpensive monocular camera. Our proposed method is based on (1) domain adaptation with an adversarial learning framework and (2) exploiting synthetic data from a simulator. To the best of the authors' knowledge, this is the first work to apply domain adaptation with adversarial networks to autonomous navigation. We present empirical results on navigation in outdoor courses using an unmanned aerial vehicle. The performance of our method is comparable to that of a supervised model with labeled real data, although our method does not require any label information for the real data. Our proposal includes a theoretical analysis that supports the applicability of our approach.

1. Introduction

Autonomous navigation for vehicles (*e.g.* self-driving cars and unmanned aerial vehicles (UAV)) has attracted great attention recently in the machine learning field. This presents great economic, social and ecological potential (Anderson & Gaston, 2013; Coifman et al., 2006; Glade, 2000). Recent advances in deep learning have garnered significant achievements (Bojarski et al., 2016). However, most prior studies required large labeled datasets, which often thwarted further progress because of the expense of human labeling.

In this paper, we propose a data-driven method for autonomous navigation that employs domain adaptation via adversarial learning networks (Ajakan et al., 2014; Shen et al., 2017) and takes only a monocular raw image as an input. Our approach has two major advantages over previous work.

First, our method alleviates the labeling issue through domain adaptation by adversarially generating realistic images from simulated images. Domain adaptation refers to adapting one domain to another so that one can use the data from the former domain to train a model for the tasks in the latter domain (Pan & Yang, 2010). We apply domain adaptation to a simulator to train a navigational model that works reasonably well in a real environment using simulated data without any real labeled data. Simulated environments do not suffer from labeling issues (Bousmalis et al., 2017). These days simulated images are often highly realistic, which attracts us to use a simulator (Straub et al., 2014) to generate training images.

Second, our method requires only a monocular camera. Many existing approaches to autonomous navigation depend on various sensors, including global positioning system (GPS) sensors and depth sensors (Geiger et al., 2012; Kim et al., 2003; Levinson et al., 2011; Urmson et al., 2008). Such approaches often raise issues. The additional cost and complexity are the main problem with using multiple sensors. They may increase the acutator burden, especially in the case of micro aerial vehicles. Additionally, sensors have their own limitations. For example, a GPS sensor does not usually operate well in an indoor environment or in a forest. Compared with other sensors, a monocular camera is light and cost-effective. Images can be acquired in real time with a camera in well-lit areas. Moreover, the latest deep learning techniques, having shown remarkable achievements in the image domain (Krizhevsky et al., 2012), may compensate for the lack of other sensors during autonomous navigation.

In the experiments presented in this paper, we show the performance of our method by navigating a UAV along trails. We succeeded in navigating the UAV automatically in three outdoor courses of up to about 300 meters by training our deep learning model using a myriad of simulator images with auto-generated labels and a few real images without any label. Our method can be applied to other vehicles as well. We also present a theoretical analysis of our method.

2. Background

2.1. Generative Adversarial Networks

Goodfellow et al. (2014) proposed generative adversarial networks (GANs), which are a popular method for synthesizing realistic data by adopting a generator, G , and a discriminator, D . G maps latent variables from the latent variable space, \mathcal{Z} , into a data space, \mathcal{X} , so that G produces

^{*}Equal contribution ¹Seoul National University, Seoul, Korea. Correspondence to: Sungroh Yoon <sryoon@snu.ac.kr>.

synthetic data to fool D . D aims to distinguish real data from the fake data generated by G . This adversarial behavior leads to the following minimax objective function:

$$\min_G \max_D \mathbb{E}_{x \sim P_r} \log D(x) + \mathbb{E}_{z \sim P_z} \log(1 - D(G(z))) \quad (1)$$

where P_r refers to a real data probability distribution defined on \mathcal{X} , and P_z refers to a latent variable distribution defined on \mathcal{Z} .

2.2. Domain Adaptation

Domain adaptation is a method that tries to adapt data from one domain (*i.e.*, the source domain) into another domain (*i.e.*, the target domain), while classification task performance is preserved in a target domain (Pan & Yang, 2010). This is considered a prior knowledge transfer of the source domain to the target domain for dealing with tasks in the target domain. Formally, we assume that there is a joint probability distribution of input data, x , with its label, y , in each domain: $P_S(x, y)$ in the source domain and $P_T(x, y)$ in the target domain. The two distributions are defined on $\mathcal{X} \times \mathcal{Y}$, where \mathcal{X} and \mathcal{Y} are the input data space and the label space, respectively. Given the labeled source domain data, $(x_s, y_s) \sim P_S(x, y)$, and unlabeled target domain data, x_t , which come from the marginal distribution, $P_T(x)$ of $P_T(x, y)$, domain adaptation learns a classifier, $h : \mathcal{X} \rightarrow \mathcal{Y}$, which properly fits on the posterior distribution, $P_T(y|x)$ of $P_T(x, y)$.

The simplest way to conduct domain adaptation is to just not care about differences in the distributions of the two domains, which are called a domain discrepancy (Long et al., 2015). It trains a model only with the source domain data and applies the model to the target domain without modifications. In many cases, this method does not work well because of the domain discrepancy (Long et al., 2015). A popular way to overcome this is to reconstruct a common representation space where the two domain distributions are projected (Ajakan et al., 2014; Long et al., 2015; Shen et al., 2017). This approach attempts to obtain a domain invariant representation space where a projected distribution is invariant from domain to domain. Additionally, it trains a model with projected data from the source domain distribution. It is considered that, as distributions of two domains on the representation space become closer, the domain discrepancy becomes smaller and the learned model performs satisfactorily on the target domain (Ajakan et al., 2014).

There are some approaches to find the common representation space. Borgwardt et al. (2006) and Huang et al. (2007) proposed methods that performed reweighting of samples from the source domain. Pan et al. (2011) and Gopalan et al. (2011) aimed to find a feature space transformation that maps a source domain distribution to a target domain distribution. While their methods attempted to match the feature distributions from the source and the target domain by reweighting and geometric transformation, there were some trials that adversarially applied a GAN framework to reconstruct the common representation space (Ajakan et al., 2014; Bousmalis et al., 2016; Shen et al., 2017). These methods focused on leading the feature represen-

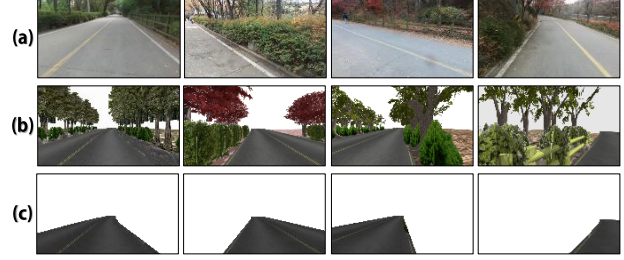


Figure 1. (a) Real images. (b) Simulator images. (c) Road masked simulator images. Images in (c) mask the road part of images in (b).

tations to be indistinguishable between the two domains while maintaining the capability of the task classifier via adversarial learning with a discriminator.

3. Method

In this section, we explain our method, which is composed of three parts, as illustrated in Fig. 2. Our objective is for a vehicle to navigate autonomously along trails, such as the one shown in the top row of Fig. 1. To achieve this without a large labeled real dataset, we train our domain adaptation model and send proper lateral/head steering commands to the vehicle using the trained model. Because we use a UAV in our experiment, we describe our method as such. The UAV can be replaced by other types of vehicles.

3.1. Domain Adaptation with Adversarial Learning

We view navigation as a multi-class classification problem. As in Smolyanskiy et al. (2017), we train a deep learning model that classifies where the UAV is located with respect to the road (*i.e.*, left/center/right-lateral class) and where the UAV heads for along the road (*i.e.*, left/straight/right-head class), based on a raw image from a camera on the UAV. Fig. 3 represents how we define lateral and head classes.

For autonomous navigation, we utilize simulator images, real images (see Fig. 1), and correct lateral/head labels for simulator images. To address the gap between simulator images and real images and the absence of labels for real images, we adopt domain adaptation with an adversarial learning framework.

We attempt to transfer a simulator image (*i.e.*, source domain) into a transferred image (*i.e.*, transferred domain) to look like a real image (*i.e.*, target domain) while maintaining characteristics of each class. Correct classification in the target domain can thus be achieved without any labels for the target domain images.

An outline of the domain adaptation model in our method is illustrated in Fig. 2, part (b). The model is composed of a transferred image generator, G_{θ_g} , a discriminator, D_{θ_d} , and a task classifier, C_{θ_c} . Our model takes target images, x^t , source images, x^s , and a noise vector, z , picked from uni-

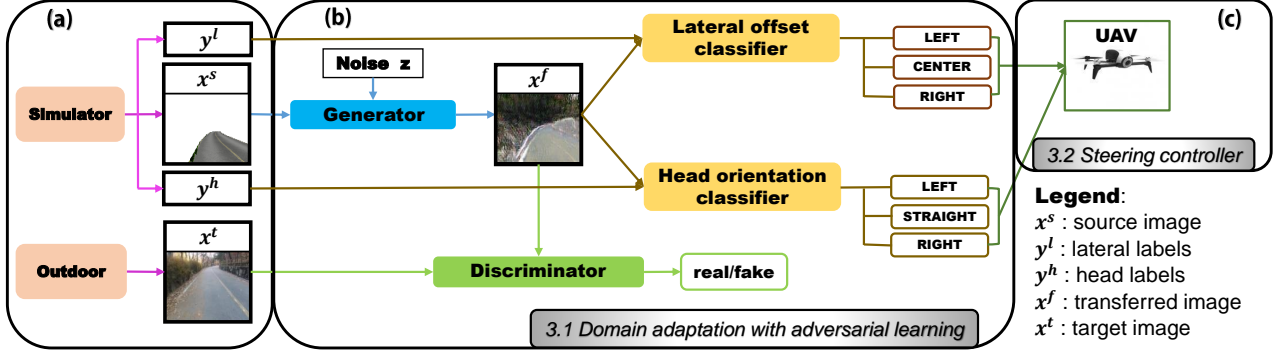


Figure 2. The overview of the proposed method.

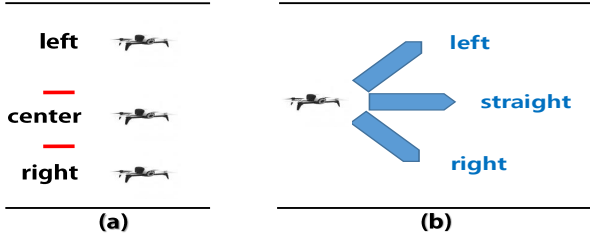


Figure 3. Illustration for (a) lateral classes and (b) head classes with respect to a road. Note that the lateral center class is slightly skewed to the right.

form distribution within $[-1, 1]^d$. d is a hyper-parameter of a noise dimension. Additionally, the lateral/head class labels, y^l, y^h , for the source images are given to the model. The generator converts a source image and the noise vector into a transferred image, x^f , which should be similar to the target image.

The discriminator takes the transferred images and the target images and distinguishes the inputs between them. The classifier takes the transferred image and the ground-truth labels of the transferred image then learns to classify the lateral and head classes of the transferred image, respectively during training. Though it is not shown in Fig. 2, the classifier takes target images then classifies their classes during the test. These three components are combined into one model, and they are trained simultaneously. No labels for target images is required. We next explain the detail object function to train the components.

3.1.1. OBJECTIVE FUNCTION

The objective function, L , for training our UAV navigation model, is as follows:

$$L = \kappa L_A + \mu L_C + \gamma L_S \quad (2)$$

where κ , μ , and γ are the weights of an adversarial loss term, L_A , a classification loss term, L_C , and a content similarity loss term, L_S , respectively.

For the adversarial loss, L_A , we adopt loss terms of the Fisher GAN (Mroueh & Sercu, 2017), inspired from Fisher linear discriminant analysis (Welling, 2005). The Fisher GAN belongs to the integral probability metrics (IPM) framework (Sriperumbudur et al., 2010), which is known to be strongly and consistently convergent (Hong et al., 2017; Sriperumbudur et al., 2009). The Fisher GAN has useful properties: it is computationally efficient, and the estimated distance is naturally bounded while maintaining stable training of the Wasserstein GAN (Arjovsky et al., 2017; Mroueh & Sercu, 2017).

The adversarial loss L_A is defined as follows:

$$L_A = \Phi(\theta_d, \theta_g) + \lambda(1 - \Omega(\theta_d, \theta_g)) - \frac{\rho}{2}(\Omega(\theta_d, \theta_g) - 1)^2 \quad (3)$$

where λ is the Lagrange multiplier and ρ is the quadratic penalty weight coefficient (Mroueh & Sercu, 2017). $\Phi(\theta_d, \theta_g)$ is the IPM equation inspired from augmented Lagrangian (Glowinski & Le Tallec, 1989) and $\Omega(\theta_d, \theta_g)$ is a constraint of the Fisher IPM metric (Hong et al., 2017; Mroueh & Sercu, 2017). $\Phi(\theta_d, \theta_g)$ and $\Omega(\theta_d, \theta_g)$ are defined as follows:

$$\Phi(\theta_d, \theta_g) = \mathbb{E}_{x \sim P_T} D_{\theta_d}(x) - \mathbb{E}_{(x,z) \sim (P_S, P_Z)} D_{\theta_d}(G_{\theta_g}(x, z)) \quad (4)$$

$$\Omega(\theta_d, \theta_g) = \frac{1}{2} (\mathbb{E}_{x \sim P_T} D_{\theta_d}^2(x) + \mathbb{E}_{(x,z) \sim (P_S, P_Z)} D_{\theta_d}^2(G_{\theta_g}(x, z))) \quad (5)$$

The classification loss term, L_C , is defined by

$$L_C = \alpha_1 l_e + \alpha_2 l_n + \alpha_3 l_p \quad (6)$$

where l_e is a soft-max cross entropy term. l_n and l_p are a negative entropy regularization term and a penalty loss term, respectively, for an extreme failure (Smolyanskiy et al., 2017). α_1 , α_2 , and α_3 refer to weights of each loss term of L_C , respectively.

The soft-max cross entropy term for our multi-class classification problem is as follows:

$$l_e = - \sum_i y_i \log(p_i) - \sum_j y_j \log(p_j) \quad (7)$$

where p_i and p_j are classifier predictions of head position, $i \in \{\text{left, straight, right}\}$, and classifier predictions of lateral position, $j \in \{\text{left, center, right}\}$, respectively. y_i and y_j are the ground truth labels of head and lateral positions, respectively.

Additionally, we add the negative entropy regularization term, l_n , and the penalty loss term, l_p , motivated by Smolyanskiy et al. (2017). l_n prevents the classifier from producing extremely sharp results. l_p penalizes the classifier so that it will not swap left and right labels of lateral and head classes, respectively. l_n and l_p are defined as follows:

$$l_n = \sum_i p_i \log(p_i) + \sum_j p_j \log(p_j) \quad (8)$$

$$l_p = p_{l/r}^{\text{head}} + p_{r/l}^{\text{head}} + p_{l/r}^{\text{lateral}} + p_{r/l}^{\text{lateral}} \quad (9)$$

where $p_{l/r}$ and $p_{r/l}$ refer to a left label prediction probability when the ground truth is right and a right label prediction probability when the ground truth is left respectively.

Because the location of a road in an image should be invariant between the source and transferred images for successful domain adaptation, we add the content similarity loss term, L_S , which guides the road part of an image to be invariant. Given the mask of the road in a simulator image, we use a masked mean squared error term for the content similarity loss term L_S as follows:

$$L_S = \mathbb{E}_{(x,z) \sim (P_S, P_Z)} \left[\frac{1}{n} \|(x - G_{\theta_g}(x, z)) \circ m\|_2^2 \right] \quad (10)$$

where n is the number of pixels of x , $\|\cdot\|_2^2$ is the squared L^2 norm, m is a binary road mask, and \circ refers to element-wise multiplication.

In the end, we optimize following equation:

$$\min_{\theta_g} \min_{\theta_c} \max_{\theta_d} \min_{\lambda} [\kappa L_A(\theta_d, \theta_g, \lambda) + \mu L_C(\theta_g, \theta_c) + \gamma L_S(\theta_g)].$$

3.2. Steering Controller

Our model gives no steering commands; it provides probabilities of each class. Thus, we need an additional steering controller module when we navigate the UAV in the inference phase. When our model provides soft-max output $[p_{\text{left}}^{\text{lateral}}, p_{\text{center}}^{\text{lateral}}, p_{\text{right}}^{\text{lateral}}]$ for the lateral classes and $[p_{\text{left}}^{\text{head}}, p_{\text{straight}}^{\text{head}}, p_{\text{right}}^{\text{head}}]$ for the head classes, our steering controller sends two velocity commands as follows:

$$\begin{aligned} v_y &= \beta_1 (p_{\text{right}}^{\text{lateral}} - p_{\text{left}}^{\text{lateral}}) \\ w_z &= \beta_2 (p_{\text{right}}^{\text{head}} - p_{\text{left}}^{\text{head}}) \end{aligned} \quad (11)$$

where v_y is a y -axis linear velocity and w_z is a z -axis angular velocity with coefficients, β_1 and β_2 . A positive y -axis linear velocity cause the UAV to move left and a positive z -axis angular velocity causes the UAV to rotate counter-clockwise. Additionally, the UAV flies forward with a constant velocity, by default. Unlike the steering controller of Smolyanskiy et al. (2017), we send the median of five successive commands to prevent abrupt behavior of the UAV.

3.3. Theoretical Analysis

We address the lack of labels in the target domain by making source images resemble target images and by giving them labels of the source images. Intuitively, if a classifier works well for the transferred images and the transferred images are similar to the target domain images, then the classifier should fit the target domain images. In this section, we show that our intuition can be explained mathematically by the upper bound of the trained model's performance under a few assumptions.

We refer to the image space and the label space as \mathcal{X} and \mathcal{Y} , respectively. For an image, $x \in \mathcal{X}$, and a label, $y \in \mathcal{Y}$, $P_T(x, y)$ and $P_F(x, y)$ defined on $\mathcal{X} \times \mathcal{Y}$ denote the joint probability on the target and the transferred domains, respectively. $P_T(x)$ and $P_T(y|x)$ are the marginal distribution and conditional probability for joint probability, $P_T(x, y)$, respectively. The same is true for $P_F(x)$ and $P_F(y|x)$. Below is the list of definitions and assumptions used in our analysis.

Definition 1. An error rate, $e(x, y)$, denotes the inaccuracy of the trained classifier for an image x and its label y . Range of the error rate is $[0, 1]$.

Definition 2. An average error in the target domain is the average error rate on the target domain; i.e.,

$$E_T = \int_{\mathcal{X} \times \mathcal{Y}} e(x, y) P_T(x, y) dx dy. \quad (12)$$

An average error in the transferred domain, E_F , is defined in the same way.¹

We can interpret E_T as the measure of the trained model's inaccuracy on the target domain. The same is true for E_F .

Assumption 3. The class information has been transferred correctly; i.e., $P_F(y|x) \approx P_T(y|x)$ in $\text{supp}(P_T) \cup \text{supp}(P_F) \subset \mathcal{X} \times \mathcal{Y}$, where $\text{supp}(\cdot)$ indicates the support of a probability distribution.

Assumption 4. The adversarial learning process has found a close solution to the global optimum.

Assumption 5. The classifier learning process on transferred domain has converged approximately to the global optimum; i.e., there is an arbitrarily small positive number $\epsilon_1 > 0$ such that $E_F < \epsilon_1$.

Assumption 3 can be supported with several practical implementations. The content loss described in Section 3.1 is an example. In a situation where we can collect labels for real images, this assumption can be removed by changing our model slightly. We discuss this situation in Section 6. Now, we suggest the following propositions using the assumptions presented above.

Proposition 6. For $P_T(x)$ and $\frac{P_T(x) + P_F(x)}{2}$, the following inequality holds:

$$TV(P_T(x) || \frac{P_T(x) + P_F(x)}{2})^2 \leq \frac{1}{4} X_2^P(P_T(x), \frac{P_T(x) + P_F(x)}{2}) \quad (13)$$

¹It should be noted that we use integral $\int \cdot$ for the discrete space \mathcal{Y} for convenience.

where TV is the total variation distance on the probability space defined by $TV(\mathbb{P}||\mathbb{Q}) = \frac{1}{2} \int |\mathbb{P} - \mathbb{Q}| d\mu$ for given measure μ and two probability distributions, \mathbb{P} and \mathbb{Q} . X_2^P is the Pearson divergence between \mathbb{P} and \mathbb{Q} .

Proof. Gibbs & Su (2002) showed that $TV(\mathbb{P}||\mathbb{Q})^2 \leq \frac{1}{4} X_2^P(\mathbb{P}, \mathbb{Q})$ holds if \mathbb{P} is dominated by \mathbb{Q} where \mathbb{P} and \mathbb{Q} are probability distributions.

Because the support of $P_T(x)$ is contained in the support of $\frac{P_T(x)+P_F(x)}{2}$, we can derive Equation 13 by substituting $P_T(x)$ for \mathbb{P} and $\frac{P_T(x)+P_F(x)}{2}$ for \mathbb{Q} . \square

Proposition 7. *There is an arbitrarily small positive number, $\epsilon_2 > 0$, such that*

$$TV(P_T(x)||P_F(x)) < 2\sqrt{\epsilon_2}. \quad (14)$$

Proof. According to Theorem 1.1 in Mroueh & Sercu (2017), the Fisher IPM is equivalent to the Chi-squared distance, $X_2^2(P_T(x), P_F(x))$.

Under Assumption 4, we could argue that there is a sufficiently small positive real number, ϵ_2 , which satisfies $X_2^2(P_T(x), P_F(x)) < \epsilon_2$. Additionally, the relationship between X_2^2 and the Pearson divergence, X_2^P , such that $X_2^2(\mathbb{P}, \mathbb{Q}) = \frac{1}{4} X_2^P(\mathbb{P}, \frac{\mathbb{P}+\mathbb{Q}}{2})$ holds (Mroueh & Sercu, 2017), gives us the following inequality:

$$\frac{1}{4} X_2^P(P_T(x), \frac{P_T(x) + P_F(x)}{2}) < \epsilon_2. \quad (15)$$

Then,

$$TV(P_T(x)||P_F(x)) = \frac{1}{2} \int |P_T(x) - P_F(x)| dx \quad (16)$$

$$= \int |P_T(x) - \frac{P_T(x)+P_F(x)}{2}| dx \quad (17)$$

$$= 2TV(P_T||\frac{P_T+P_F}{2}) < 2\sqrt{\epsilon_2}. \quad (18)$$

The inequality of Eq. 18 comes from Prop. 6 and Eq. 15. \square

The average error of the classifier on the target domain can be guaranteed to be sufficiently small under the above assumptions and Prop. 7 as follows:

$$E_T = \int_{\mathcal{X} \times \mathcal{Y}} e(x, y) P_T(x, y) dx dy \quad (19)$$

$$= \int_{\mathcal{X} \times \mathcal{Y}} e(x, y) (P_T(x, y) - P_F(x, y) + P_F(x, y)) dx dy \quad (20)$$

$$\leq \int_{\mathcal{X} \times \mathcal{Y}} e(x, y) |P_T(x, y) - P_F(x, y)| dx dy + E_F \quad (21)$$

$$\leq \int_{\mathcal{X} \times \mathcal{Y}} |P_T(x) P_T(y|x) - P_F(x) P_F(y|x)| dx dy + E_F \quad (22)$$

$$\approx \int_{\mathcal{X}} |P_T(x) - P_F(x)| dx \int_{\mathcal{Y}} P_T(y|x) dy + E_F \quad (23)$$

$$= 2TV(P_T||P_F) + E_F < 4\sqrt{\epsilon_2} + \epsilon_1 \quad (24)$$

where we apply $e(x, y) \leq 1$ to Eq. 22, and Assumption 3 to Eq. 23.

As ϵ_1 and ϵ_2 are sufficiently small, the error on the target domain should also be small. This analysis explains that

why our empirical results in the next section show excellent performance. The mathematical flow of Eq. 19-24 resembles that of Ross et al. (2013), but can be considered a special case with one time-step.

4. Experiment

4.1. Setup

We generated around 8000 images for each lateral and head class by randomizing the position of the UAV in the simulator and by fixing the titled angle by -45,0,45 degrees, with respect to the road. Aside from the simulator images for the source images, we gathered around total 30,000 images for the target images by recording on a local mountain trail. In both cases, we fixed the altitude of UAV to approximately 1.5 m.

We used the parrot Bebop2 drone for our experiment. To send a command from the trained model to a drone, we utilized parrot Bebop ROS package² with a joystick connection.³ We implemented our UAV navigation system with Tensorflow (Abadi et al., 2016). During the test, we calculated our model's output every 50ms with NVIDIA GTX 1060. We set our commanding interval to every 1 second to protect pedestrians.

As shown in Fig. 1, we built two kinds of source images. One contains a road and a background, such as trees and sky. The other contains only a road and the other area is masked with zeros as shown in the bottom row of Fig. 1. We denote the former as a unmasked source image and the latter as a masked source image. During the experiment, we found that the performance of the model with unmasked source images was worse and less robust than the model with masked source images. We thus used the masked source images afterwards. Our source image building methods is described in the supplementary material.

4.2. Off-line Test Results

We conducted off-line tests for our trained model prior to testing outside. We not only measured classification accuracy, we also monitored steering commands on the test target domain data which was not used in the training phase. We checked both because the navigation depends on steering commands, not on classification accuracy. Because our approach focuses on using a simulator and unlabeled real data, not the architecture of the model, we compared our model to a supervised learning (SL) model with source domain data and another with target domain data.

Tab. 1 lists the off-line test results (see captions for detail). Our model succeeded in giving correct commands in all cases, as like the target image SL model, whereas both source SL models failed. Furthermore, even though classification accuracies of some classes listed in Tab. 1a were relatively low in our model's result, the UAV could reason-

² Available at <http://bebop-autonomy.readthedocs.io/en/latest>

³ We activated joystick steering only when a drone was stuck into a dangerous position.

Table 1. The off-line test result. Source image supervised model (SL) model is supervised-trained with unmasked source images. The source mask SL model is supervised-trained with masked source images. The target image SL model is supervised-trained with real images and their lateral/head labels. The steering commands for images having a left/straight/right lateral label and a left/center/right head label should be negative, zero, and positive, respectively. The light gray shaded cell in Tab. 1b, represents the steering command with the correct sign for left and right labels and the dark gray cells incorrect sign. As absolute values of a steering command get larger, the UAV experiences sharper movements.

(a) Classification accuracy

Model	Lateral offset label			Head orientation label		
	left	center	right	left	straight	right
Source image SL	0.0 %	65.5 %	55.2 %	76.8 %	64.1 %	45.0 %
Source mask SL	31.4 %	0.0 %	30.3 %	1.7 %	45.2 %	46.4 %
Target image SL	90.1 %	99.8 %	55.4 %	91.7 %	100.0 %	96.9 %
Our model	92.0 %	52.8 %	46.5 %	70.6 %	55.8 %	57.7 %

(b) Average steering command

Model	Lateral offset label			Head orientation label		
	left	center	right	left	straight	right
Source image SL	0.07±0.19	0.35±0.40	0.55±0.44	-0.70±0.52	0.09±0.55	0.04±0.89
Source mask SL	0.35±0.83	-0.28±0.79	-0.32±0.75	0.29±0.34	0.52±0.29	0.57±0.28
Target image SL	-0.83±0.22	0.002±0.04	0.52±0.37	-0.89±0.23	-0.004±0.01	0.94±0.16
Our model	-0.87±0.37	-0.14±0.59	0.31±0.66	-0.68±0.46	0.03±0.59	0.40±0.70

ably move because a steering command with a correct sign guides it to move properly. One may argue that the probability of a right lateral in the target image SL model is lower than other classes in Tab. 1a. Although we have another target image SL model which has 99 % accuracy in the right lateral label, this model performed worse on outdoor navigation than the target image SL model of Tab. 1a.

Additionally, one may argue that transferred images should look like target images to succeed in navigation. Fig. 4 shows the source images and corresponding transferred images. Target images are chosen for their similarity to each transferred image of the same column.

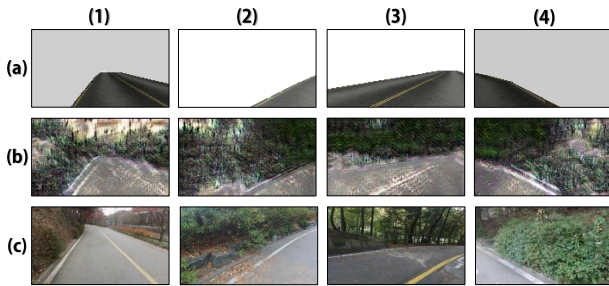


Figure 4. Each row represents (a) source images, (b) transferred images, and (c) target images. Each column shows images with label (1) lateral left/head straight, (2) lateral left/head left, (3) lateral center/head left, and (4) lateral center/head right. More images are shown in the supplementary materials.

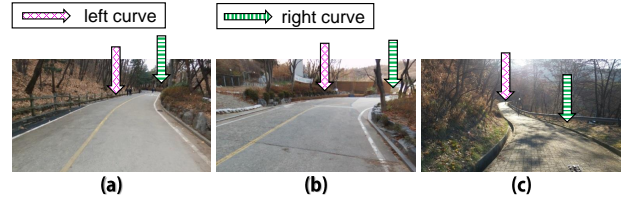


Figure 5. Test courses. (a) Course 1: two slight corners. (b) Course 2: two sharp curves, unseen street during the training phase. (c) Course 3: different environment, not asphalt but sidewalk road with two corners.

4.3. Outdoor Navigation On-line Test Results

In the outdoor on-line test, we verified the performance of our approach based on two criteria, as is commonly carried out in this field (Smolyanskiy et al., 2017). First, we ask, "how many human interrupts are required to finish navigation in certain trail courses?" to see navigation performance. Second, we ask, "how well UAV recovers from intentional disturbance?" to see the ability to handle unexpected situation. Because the source mask SL model showed the lowest performance in the off-line test, we omitted that case from navigation results.

4.3.1. AUTONOMOUS NAVIGATION

We tested our model on three courses. The length of each was approximately 190 m, 60 m, and 110 m, respectively. Course 1 in Fig. 5, where we gathered real images, has relatively slight curves. Courses 2 and 3, where we did not gather images, have more sharp curves compared to Course 1. We argue that tests on these three courses were appro-

priate to demonstrate the effectiveness of our model. We observed not only navigation performance but also robustness of our model by testing on the course of which scene was used during training (*i.e.*, Course 1) and courses unseen prior (*i.e.*, Courses 2 and 3) even with different environments.

Tab. 2 shows the average number of human interrupts until the UAV finished each course with three models. The source image SL models failed to finish the course within reasonable trials. We omitted the performance of source image SL on Courses 2 and 3, because Course 1 could be regarded as the easiest course. Our model showed successful performance compared to the target image SL model. Additionally, the UAV navigated without a human interrupt for 270 m, but it could have gone farther if we had not terminated navigation.

Given the performance of the source image SL models, we could conclude that applying the model trained only with the simulator data into outdoor environment is prone to failure. This means that domain adaptation is essential. Our UAV navigation video is available at <https://www.youtube.com/watch?v=MKi0SJ4YjLs&t=3s>.

Table 2. Average number of human interrupts to finish. We counted the total number of interrupts in five navigation trials on each course. Our model showed comparable performance with a target image SL model.

	Course 1	Course 2	Course 3
Source image SL	> 10	.	.
Target image SL	0.2 (1/5)	1.2 (6/5)	0.2 (1/5)
Our model	0.8 (4/5)	1.4 (7/5)	0.0 (0/5)

4.3.2. RECOVERY FROM DISTURBANCE

We tested our model for successful recovery from disturbances. A vehicle should avoid objects, including humans. In the case of a UAV, the wind blows in the outdoor and strong air currents are caused by the UAV, itself. Thus, UAVs tend to lose stability and deviate from the desirable location or path. It is very important to recover from these deviations during autonomous navigation. We placed the UAV in a non-desirable position intentionally to measure its ratio of successful returns to the desired position. Tab. 3 shows the ratios in extreme cases (*i.e.*, lateral left/head left and lateral right/head right). We set 20 undesirable positions for each case and measured the number of UAV that returned to the normal path (*i.e.*, lateral center/head straight) in a reasonable time. Our model successfully recovered as much as the target SL model.

5. Related Work

Non-learning-based approaches for autonomous navigation have shown impressive maneuvers (Geiger et al., 2012; Kushleyev et al., 2013; Mellinger & Kumar, 2011; Mellinger et al., 2012; Shen et al., 2011; Urmson et al., 2008; Zingg et al., 2010). However, these methods have

Table 3. Success rate to recover. We counted the number of successful recoveries after 20 intentional disturbances at extreme cases. Left/left and right/right refer to lateral left/head left and lateral right/head right, respectively.

	left/left	right/right
Target image SL	95 % (19/20)	60 % (12/20)
Our model	95 % (19/20)	60 % (12/20)

additional requirements, such as state feedback and state extraction from raw inputs with other sensors or computationally expensive systems, which are incompatible with our purpose. However, learning-based methods or data-driven methods produce a reactive controller by mapping raw inputs into an action. Data-driven methods are also known to seek a robust solution (Bohg et al., 2014).

Supervised learning based methods have been proposed to perform **autonomous navigation using real images**. Ross et al. (2013) and Kahn et al. (2016) adopted DAGGER, and GPS (Levine & Koltun, 2013) respectively. Each group implemented a variant of SL to navigate UAVs in the outdoor environment. Although Kahn et al. (2016) applied their own method to a simulator, it may be straightforward to extend their method to a real environment. Bojarski et al. (2016) achieved autonomous highway driving using the basic supervised method. Zhang & Cho (2016), Xu et al. (2016) and Codevilla et al. (2017) improved basic supervised methods for a car and remote-control car driving. A supervised method proposed by Chen et al. (2015) matched images to predefined affordances instead of an exact action. Giusti et al. (2016) and Smolyanskiy et al. (2017) suggested viewing navigation as a classification problem instead of a regression problem.

These approaches have a limitation, that acquiring labels for real images is laborious or expensive. It causes these methods to be less applicable to various environments. Although Kahn et al. (2016) automated the labeling process, they still needed additional information that is difficult to acquire in the outdoor environment with only a monocular camera. We addressed this limitation by utilizing a simulator and by not applying SL on the real image domain.

Using a simulator for training an autonomous navigation system has advantages. One can measure any physical property, including location and velocity in freedom. One need not care about damage to a vehicle. However, there is a domain discrepancy issue. To address this issue, Mirowski et al. (2016) exploited a depth image, which is more invariant across the two environments. They used a reconstructed depth from a 2D image or a depth sensor to obtain the depth image. Sadeghi & Levine (2016) suggested randomization be applied to the simulator with highly various features, such as light conditions, textures, and objects. They showed that their navigation model worked reasonably well in an indoor environment although they did not provide any real images during the training.

However, using a depth sensor increases the cost. Reconstructing a depth image incurs additional error and high computing cost. The indoor environment is also relatively

simple and plain, compared to the outdoors. Thus, it remains doubtful whether the method proposed by Sadeghi & Levine (2016) would work satisfactorily in the outdoors. In this paper, we take advantage of the simulator, solving domain discrepancy by domain adaptation with an adversarial learning framework.

Domain adaptation has been applied in many tasks. Dafttry et al. (2016) learned transferable policies for the UAV navigation using domain adaptation. They tried to decrease domain discrepancy defined with maximum mean discrepancy (MMD) (Gretton et al., 2012a) of a predefined kernel. MMD has shown its applicability in various tasks (Dziugaite et al., 2015; Kim & Pineau, 2013; Pan et al., 2008), yet is still highly dependent on the choice of the kernel (Li et al., 2017) and may result in biased estimation, because of the sampling variance (Gretton et al., 2012b). Bousmalis et al. (2017) and Shrivastava et al. (2016) used a simulator for domain adaptation with an adversarial learning framework. Bousmalis et al. (2017) adopted this framework for a grasping task. Shrivastava et al. (2016) refined eye rendered images to be more realistic by using GANs. With images generated by a refined renderer, (Shrivastava et al., 2016) gained the higher performance via eye-gaze estimation.

6. Discussion

We succeeded in navigating a UAV automatically without any labels for real images. To the best of the authors' knowledge, this is the first attempt to apply domain adaptation with adversarial learning to an autonomous vehicle navigation task. This approach may extend the scope of autonomous navigation to various outdoor environments that can be simulated. Additionally, we showed the potential robustness of our approach by demonstrating reasonable navigation performance in courses where no scene was used during training.

In Section 3.3, we analyzed the performance of our model. We assumed that successful adversarial learning leads to the distribution of transferred images and the distribution of real images being close to each other. Though the visual images in Fig. 4 support our assumption, we showed the similarity between the two distributions by embedding images from each to a low dimensional space, using t-SNE (Maaten & Hinton, 2008).⁴ Fig. 6 shows the embedded points for various images. The transferred images were closer to the real images than the source images, supporting our assumption.

We made a slightly strong assumption (*i.e.*, Assumption 3). Thus, we considered the case in which we could remove the assumption. If we can collect labeled real images, an adversarial learning module can take not only images but also their labels as an input. With two other assumptions, we can replace all marginal distributions of Prop. 6 and 7 with joint distribution of image x and label y without mod-

⁴Figures by other embedding methods such as PCA, kernel PCA are displayed in the supplementary material.

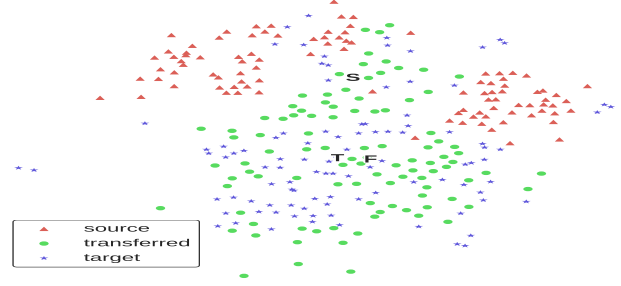


Figure 6. t-SNE result. 'S', 'F' and 'T' indicate the median of source images, transferred images and target images, respectively.

ifying the conclusion. In this case, although we use labels for real images, we may still benefit from our approach in terms of performance. Bousmalis et al. (2017) showed the improvement of the success rate in a grasping task by using domain adaptation with real labeled data.

We partly adopted the method by Bousmalis et al. (2016); however, we took a different approach from Bousmalis et al. (2016) in that we did not adopt the content similarity loss term, L_S , in the training phase (*i.e.*, $\gamma = 0$ in Eq. 2). We tested models with L_S but these cases caused the transferred images to remain highly similar to the source images, resulting in feeble performance in the off-line test. We instead masked a simulator image on the road part. Our model, with masked source image without L_S , could still keep the location of the road as shown in Fig. 4. This was in line with the objective of the similarity term and Assumption 3.

Despite our successful results, there were some failure cases. First, our model was slightly non-robust to weather conditions such as strong sunlight, mist, and snow. We collected real images during the hours of 3-5 pm in the fall and winter. Thus, almost all images were exposed to small amounts of sunlight. Thus, the transferred image was necessarily biased to the similar state. When the sun was strong, the road in a real image changed its color from gray to yellow, causing navigation to fail. To be robust to weather conditions, many images under various conditions may be required.

Second, both our model and the target image SL model failed when branches from trees protruded the road from above. Though a UAV was on the road, protruding branches collided with the wing of the UAV, leading to failure. Because the road remained visible through pine leaves, it was difficult for the UAV to avoid those obstacles. Solving these problems will be future work.

Although we used a UAV to validate our method of autonomous navigation, it would be possible to apply our method to other types of vehicles. The task we conducted in this study is a version of lane-tracking, which is one of many components of autonomous driving. As we have shown with the validity of our method to use a simulator in autonomous navigation, we are planning to perform more complex navigation tasks by expanding our method and in-

corporating other machine learning techniques, including reinforcement learning.

7. Conclusion

In this paper, we applied domain adaptation with adversarial learning for autonomous navigation. Our model showed satisfactory performance without any labels for real images. We discovered the possibility of truly autonomous navigation in various environments using enormous and accessible simulator images. We summarize our contributions as follows:

- We successfully performed autonomous UAV navigation in three courses with real images in an unsupervised manner. To the best of the authors' knowledge, this is the first work that applies domain adaptation with adversarial learning networks to autonomous navigation.
- We built the simulator to be used in the domain adaptation framework. By combining domain adaptation with our simulator and classification view on the navigation, we improved previous methods in terms of data efficiency (*i.e.*, we resolved the labeling issue).
- We also provided a theoretical analysis that showed why our method works, despite the absence of labels.

References

- Abadi, Martín, Agarwal, Ashish, Barham, Paul, Brevdo, Eugene, Chen, Zhifeng, Citro, Craig, Corrado, Greg S, Davis, Andy, Dean, Jeffrey, Devin, Matthieu, et al. Tensorflow: Large-scale machine learning on heterogeneous distributed systems. *arXiv preprint arXiv:1603.04467*, 2016.
- Ajakan, Hana, Germain, Pascal, Larochelle, Hugo, Laviolette, François, and Marchand, Mario. Domain-adversarial neural networks. *arXiv preprint arXiv:1412.4446*, 2014.
- Anderson, Karen and Gaston, Kevin J. Lightweight unmanned aerial vehicles will revolutionize spatial ecology. *Frontiers in Ecology and the Environment*, 11(3): 138–146, 2013.
- Arjovsky, Martin, Chintala, Soumith, and Bottou, Léon. Wasserstein gan. *arXiv preprint arXiv:1701.07875*, 2017.
- Bohg, Jeannette, Morales, Antonio, Asfour, Tamim, and Kragic, Danica. Data-driven grasp synthesis: a survey. *IEEE Transactions on Robotics*, 30(2):289–309, 2014.
- Bojarski, Mariusz, Del Testa, Davide, Dworakowski, Daniel, Firner, Bernhard, Flepp, Beat, Goyal, Praseem, Jackel, Lawrence D, Monfort, Mathew, Muller, Urs, Zhang, Jiakai, et al. End to end learning for self-driving cars. *arXiv preprint arXiv:1604.07316*, 2016.
- Borgwardt, Karsten M, Gretton, Arthur, Rasch, Malte J, Kriegel, Hans-Peter, Schölkopf, Bernhard, and Smola, Alex J. Integrating structured biological data by kernel maximum mean discrepancy. *Bioinformatics*, 22(14): e49–e57, 2006.
- Bousmalis, Konstantinos, Silberman, Nathan, Dohan, David, Erhan, Dumitru, and Krishnan, Dilip. Unsupervised pixel-level domain adaptation with generative adversarial networks. *arXiv preprint arXiv:1612.05424*, 2016.
- Bousmalis, Konstantinos, Irpan, Alex, Wohlhart, Paul, Bai, Yunfei, Kelcey, Matthew, Kalakrishnan, Mrinal, Downs, Laura, Ibarz, Julian, Pastor, Peter, Konolige, Kurt, et al. Using simulation and domain adaptation to improve efficiency of deep robotic grasping. *arXiv preprint arXiv:1709.07857*, 2017.
- Chen, Chenyi, Seff, Ari, Kornhauser, Alain, and Xiao, Jianxiong. Deepdriving: Learning affordance for direct perception in autonomous driving. In *Computer Vision (ICCV), 2015 IEEE International Conference on*, pp. 2722–2730. IEEE, 2015.
- Codevilla, Felipe, Müller, Matthias, Dosovitskiy, Alexey, López, Antonio, and Koltun, Vladlen. End-to-end driving via conditional imitation learning. *arXiv preprint arXiv:1710.02410*, 2017.
- Coifman, Benjamin, McCord, Mark, Mishalani, Rabi G, Iswalt, Michael, and Ji, Yuxiong. Roadway traffic monitoring from an unmanned aerial vehicle. In *IEEE Proceedings-Intelligent Transport Systems*, volume 153, pp. 11–20. IET, 2006.
- Daftry, Shreyansh, Bagnell, J Andrew, and Hebert, Martial. Learning transferable policies for monocular reactive mav control. In *International Symposium on Experimental Robotics*, pp. 3–11. Springer, 2016.
- Dziugaite, Gintare Karolina, Roy, Daniel M, and Ghahramani, Zoubin. Training generative neural networks via maximum mean discrepancy optimization. *arXiv preprint arXiv:1505.03906*, 2015.
- Geiger, Andreas, Lenz, Philip, and Urtasun, Raquel. Are we ready for autonomous driving? the kitti vision benchmark suite. In *Computer Vision and Pattern Recognition (CVPR), 2012 IEEE Conference on*, pp. 3354–3361. IEEE, 2012.
- Gibbs, Alison L and Su, Francis Edward. On choosing and bounding probability metrics. *International statistical review*, 70(3):419–435, 2002.
- Giusti, Alessandro, Guzzi, Jérôme, Cireşan, Dan C, He, Fang-Lin, Rodríguez, Juan P, Fontana, Flavio, Faessler, Matthias, Forster, Christian, Schmidhuber, Jürgen, Di Caro, Gianni, et al. A machine learning approach to visual perception of forest trails for mobile robots. *IEEE Robotics and Automation Letters*, 1(2): 661–667, 2016.

- Glade, David. Unmanned aerial vehicles: Implications for military operations. Technical report, Air Univ Press Maxwell Afb Al, 2000.
- Glowinski, Ronald and Le Tallec, Patrick. *Augmented Lagrangian and operator-splitting methods in nonlinear mechanics*, volume 9. SIAM, 1989.
- Goodfellow, Ian, Pouget-Abadie, Jean, Mirza, Mehdi, Xu, Bing, Warde-Farley, David, Ozair, Sherjil, Courville, Aaron, and Bengio, Yoshua. Generative adversarial nets. In *Advances in neural information processing systems*, pp. 2672–2680, 2014.
- Gopalan, Raghuraman, Li, Ruonan, and Chellappa, Rama. Domain adaptation for object recognition: An unsupervised approach. In *Computer Vision (ICCV), 2011 IEEE International Conference on*, pp. 999–1006. IEEE, 2011.
- Gretton, Arthur, Borgwardt, Karsten M, Rasch, Malte J, Schölkopf, Bernhard, and Smola, Alexander. A kernel two-sample test. *Journal of Machine Learning Research*, 13(Mar):723–773, 2012a.
- Gretton, Arthur, Borgwardt, Karsten M, Rasch, Malte J, Schölkopf, Bernhard, and Smola, Alexander. A kernel two-sample test. *Journal of Machine Learning Research*, 13(Mar):723–773, 2012b.
- Hong, Yongjun, Hwang, Uiwon, Yoo, Jaeyoon, and Yoon, Sungroh. How generative adversarial nets and its variants work: An overview of gan. *arXiv preprint arXiv:1711.05914*, 2017.
- Huang, Jiayuan, Gretton, Arthur, Borgwardt, Karsten M, Schölkopf, Bernhard, and Smola, Alex J. Correcting sample selection bias by unlabeled data. In *Advances in neural information processing systems*, pp. 601–608, 2007.
- Kahn, Gregory, Zhang, Tianhao, Levine, Sergey, and Abbeel, Pieter. Plato: Policy learning using adaptive trajectory optimization. *arXiv preprint arXiv:1603.00622*, 2016.
- Kim, Beomjoon and Pineau, Joelle. Maximum mean discrepancy imitation learning. In *Robotics: Science and systems*, 2013.
- Kim, Jong-Hyuk, Sukkarieh, Salah, and Wishart, Stuart. Real-time navigation, guidance, and control of a uav using low-cost sensors. In *Field and Service Robotics*, pp. 299–309. Springer, 2003.
- Koenig, Nathan and Howard, Andrew. Design and use paradigms for gazebo, an open-source multi-robot simulator. In *IEEE/RSJ International Conference on Intelligent Robots and Systems*, pp. 2149–2154, Sendai, Japan, Sep 2004.
- Krizhevsky, Alex, Sutskever, Ilya, and Hinton, Geoffrey E. Imagenet classification with deep convolutional neural networks. In *Advances in neural information processing systems*, pp. 1097–1105, 2012.
- Kushleyev, Alex, Mellinger, Daniel, Powers, Caitlin, and Kumar, Vijay. Towards a swarm of agile micro quadrotors. *Autonomous Robots*, 35(4):287–300, 2013.
- Levine, Sergey and Koltun, Vladlen. Guided policy search. In *Proceedings of the 30th International Conference on Machine Learning (ICML-13)*, pp. 1–9, 2013.
- Levinson, Jesse, Askeland, Jake, Becker, Jan, Dolson, Jennifer, Held, David, Kammel, Soeren, Kolter, J Zico, Langer, Dirk, Pink, Oliver, Pratt, Vaughan, et al. Towards fully autonomous driving: Systems and algorithms. In *Intelligent Vehicles Symposium (IV), 2011 IEEE*, pp. 163–168. IEEE, 2011.
- Li, Chun-Liang, Chang, Wei-Cheng, Cheng, Yu, Yang, Yiming, and Póczos, Barnabás. Mmd gan: Towards deeper understanding of moment matching network. *arXiv preprint arXiv:1705.08584*, 2017.
- Long, Mingsheng, Cao, Yue, Wang, Jianmin, and Jordan, Michael. Learning transferable features with deep adaptation networks. In *International Conference on Machine Learning*, pp. 97–105, 2015.
- Maaten, Laurens van der and Hinton, Geoffrey. Visualizing data using t-sne. *Journal of Machine Learning Research*, 9(Nov):2579–2605, 2008.
- Mellinger, Daniel and Kumar, Vijay. Minimum snap trajectory generation and control for quadrotors. In *Robotics and Automation (ICRA), 2011 IEEE International Conference on*, pp. 2520–2525. IEEE, 2011.
- Mellinger, Daniel, Michael, Nathan, and Kumar, Vijay. Trajectory generation and control for precise aggressive maneuvers with quadrotors. *The International Journal of Robotics Research*, 31(5):664–674, 2012.
- Mirowski, Piotr, Pascanu, Razvan, Viola, Fabio, Soyer, Hubert, Ballard, Andy, Banino, Andrea, Denil, Misha, Goroshin, Ross, Sifre, Laurent, Kavukcuoglu, Koray, et al. Learning to navigate in complex environments. *arXiv preprint arXiv:1611.03673*, 2016.
- Mroueh, Youssef and Sercu, Tom. Fisher gan. *arXiv preprint arXiv:1705.09675*, 2017.
- Pan, Sinno Jialin and Yang, Qiang. A survey on transfer learning. *IEEE Transactions on knowledge and data engineering*, 22(10):1345–1359, 2010.
- Pan, Sinno Jialin, Kwok, James T, and Yang, Qiang. Transfer learning via dimensionality reduction. In *AAAI*, volume 8, pp. 677–682, 2008.
- Pan, Sinno Jialin, Tsang, Ivor W, Kwok, James T, and Yang, Qiang. Domain adaptation via transfer component analysis. *IEEE Transactions on Neural Networks*, 22(2):199–210, 2011.

- Ross, Stéphane, Melik-Barkhudarov, Narek, Shankar, Kumar Shaurya, Wendel, Andreas, Dey, Debadeepta, Bag-nell, J Andrew, and Hebert, Martial. Learning monocular reactive uav control in cluttered natural environments. In *Robotics and Automation (ICRA), 2013 IEEE International Conference on*, pp. 1765–1772. IEEE, 2013.
- Sadeghi, Fereshteh and Levine, Sergey. *cad²rl*: Real single-image flight without a single real image. *arXiv preprint arXiv:1611.04201*, 2016.
- Schölkopf, Bernhard, Smola, Alexander, and Müller, Klaus-Robert. Kernel principal component analysis. In *International Conference on Artificial Neural Networks*, pp. 583–588. Springer, 1997.
- Shen, Jian, Qu, Yanru, Zhang, Weinan, and Yu, Yong. Ad-versarial representation learning for domain adaptation. *arXiv preprint arXiv:1707.01217*, 2017.
- Shen, Shaojie, Michael, Nathan, and Kumar, Vijay. Au-tonomous multi-floor indoor navigation with a compu-tationally constrained mav. In *Robotics and automation (ICRA), 2011 IEEE international conference on*, pp. 20–25. IEEE, 2011.
- Shrivastava, Ashish, Pfister, Tomas, Tuzel, Oncel, Susskind, Josh, Wang, Wenda, and Webb, Russ. Learn-ing from simulated and unsupervised images through adversarial training. *arXiv preprint arXiv:1612.07828*, 2016.
- Smolyanskiy, Nikolai, Kamenev, Alexey, Smith, Jeffrey, and Birchfield, Stan. Toward low-flying autonomous mav trail navigation using deep neural networks for envi-ronmental awareness. *arXiv preprint arXiv:1705.02550*, 2017.
- Sriperumbudur, Bharath K, Fukumizu, Kenji, Gretton, Arthur, Schölkopf, Bernhard, and Lanckriet, Gert RG. On integral probability metrics, ϕ -divergences and bi-nary classification. *arXiv preprint arXiv:0901.2698*, 2009.
- Sriperumbudur, Bharath K, Gretton, Arthur, Fukumizu, Kenji, Schölkopf, Bernhard, and Lanckriet, Gert RG. Hilbert space embeddings and metrics on probability measures. *Journal of Machine Learning Research*, 11 (Apr):1517–1561, 2010.
- Straub, Carrie, Dieker, Lisa, Hughes, Charles, and Hynes, Michael. Mixed-reality computer simulation: A new paradigm for higher education. In *Presentation deliv-ered at the Conference on Higher Education Pedagogy Conference on higher education pedagogy*, 2014.
- Tenenbaum, Joshua B, De Silva, Vin, and Langford, John C. A global geometric framework for nonlinear di-mensionality reduction. *science*, 290(5500):2319–2323, 2000.
- Urmson, Chris, Anhalt, Joshua, Bagnell, Drew, Baker, Christopher, Bittner, Robert, Clark, MN, Dolan, John, Duggins, Dave, Galatali, Tugrul, Geyer, Chris, et al. Au-tonomous driving in urban environments: Boss and the urban challenge. *Journal of Field Robotics*, 25(8):425–466, 2008.
- Welling, Max. Fisher linear discriminant analysis. *Depart-ment of Computer Science, University of Toronto*, 3(1), 2005.
- Wold, Svante, Esbensen, Kim, and Geladi, Paul. Princi-pal component analysis. *Chemometrics and intelligent laboratory systems*, 2(1-3):37–52, 1987.
- Xu, Huazhe, Gao, Yang, Yu, Fisher, and Darrell, Trevor. End-to-end learning of driving models from large-scale video datasets. *arXiv preprint*, 2016.
- Zhang, Jiakai and Cho, Kyunghyun. Query-efficient imita-tion learning for end-to-end autonomous driving. *arXiv preprint arXiv:1605.06450*, 2016.
- Zingg, Simon, Scaramuzza, Davide, Weiss, Stephan, and Siegwart, Roland. Mav navigation through indoor cor-ridors using optical flow. In *Robotics and Automation (ICRA), 2010 IEEE International Conference on*, pp. 3361–3368. IEEE, 2010.

Supplementary Material

We built our simulator environment using Gazebo (Koenig & Howard, 2004), a widely known robot simulator. Because our navigation model targeted a local road made of asphalt surrounded by bushes and tall trees, we built a simulated environment that was similar to the targeted real environment.

We built our simulator environment in two phases. First, we generated various curved and straight roads. By determining the roads' curvatures and length according to our heuristic road generator, described later, we obtained coordinates of natural trails to be rendered. We then created many objects, such as a maple tree, a ginkgo tree, bushes, fences, etc., using an open source CAD tool Blender. We arranged these objects along the road, randomly.

We now describe our heuristic road generator mentioned above. A road generator aimed to produce the coordinates of natural looking trails like the one we targeted, which were to be rendered in a simulator. Fig. S1 shows the generated road coordinates by the road generator.

Fig. S2 illustrates its process. By determining each road segment's curvature, θ , and length, l , we created road coordinates to be rendered in the simulator. Negative θ_1, θ_2 , and θ_3 , in Fig. S2, result in a right-curved trail. A positive angle goes counter-clockwise.



Figure S1. The randomly generated diverse road coordinate to be rendered in the simulator.

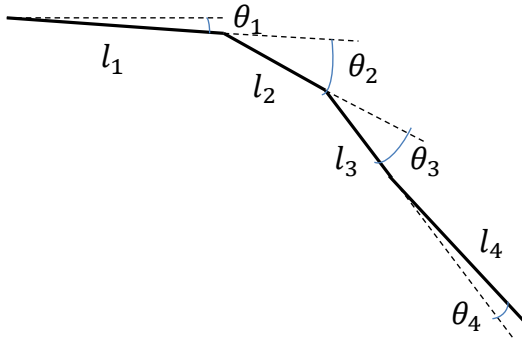


Figure S2. Road generator determines the curvature θ and length l of each road segments.

More detailed road generator procedures are described in Algorithm S1. The procedure was designed for curved roads to have relatively uniform curvature and smoothness

("else" part). We also set a relatively long straight path to appear after a road curves more than a predefined angle ("if" part). All numbers in Algorithm S1 are arbitrary.

Algorithm S1 Heuristic road generator

```

curved_angle = 0°, i = 0
repeat
  if i == 1 or  $\theta_{i-1} < 10^\circ$  or curved_angle > 45°
  then
    curved_angle = 0°
    pick up  $\theta_i \sim \mathcal{N}(0^\circ, 5^\circ)$ 
     $l_i = 5m$ 
  else
    pick up  $\theta_i \sim \mathcal{N}(\theta_{i-1}, 2^\circ)$ 
     $l_i = 1m$ 
  end if
  curved_angle  $\leftarrow$  curved_angle +  $\theta_i$ 
  i  $\leftarrow$  i + 1
until a generated road pass some boundaries
    
```

S1. Additional Transferred Images

We show additional transferred images for each lateral/head label in Figure S3. Figure S3 displays source images, transferred images and target images, from left-to-right, with corresponding labels described in the box. The transferred images look like the target images, whereas road information from source image was maintained.

S2. Embedding by Other Methods

We conducted other embedding methods to see if the transferred images really became similar to the target images, like the one we show in the discussion section. We used isomap (Tenenbaum et al., 2000), principal component analysis (PCA) (Wold et al., 1987) and kernel PCA (Schölkopf et al., 1997). We also showed t-SNE results having more points (i.e., 1,000 per domain). Figure S4, S5, S6, and S7 represent the embedding results by isomap, PCA, PCA with polynomial kernel and t-SNE each. The transferred images moved toward target images in all figures. S, T, and F in each figure, indicate the median of source, transferred, and target domain embedding images, respectively.

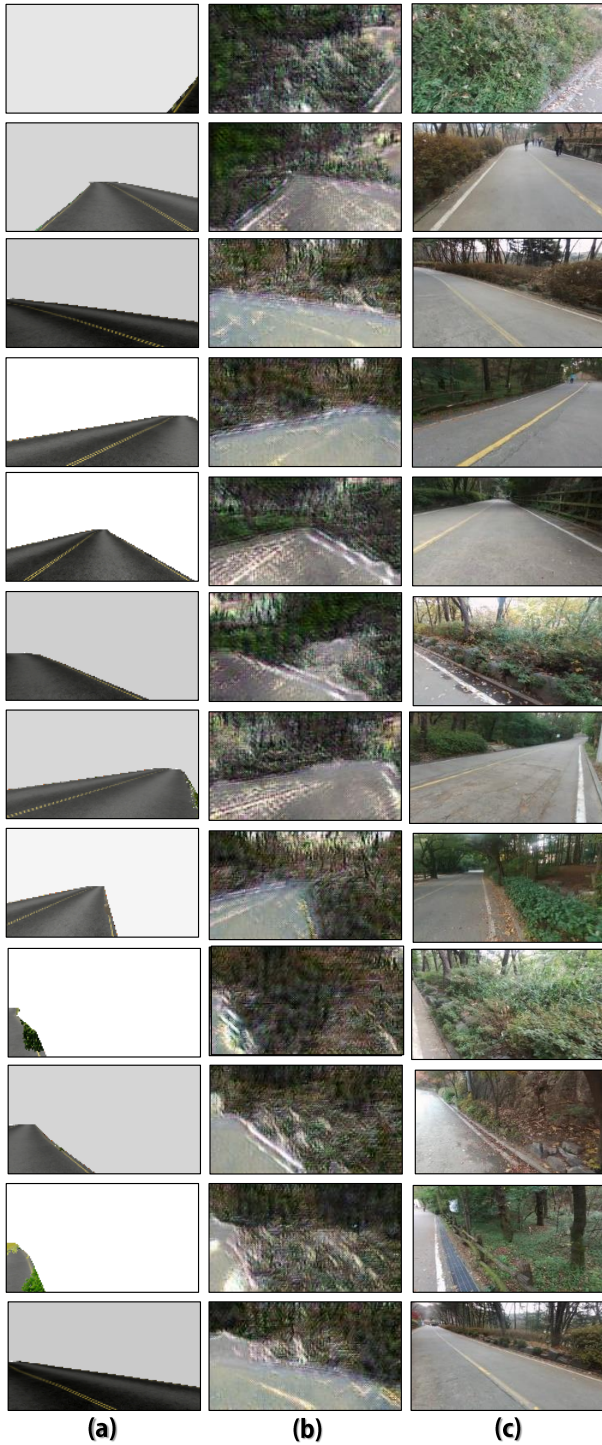


Figure S3. (a) Source images. (b) Transferred images. (c) Target images. Note that target images are chosen to be the most similar ones to transferred images.

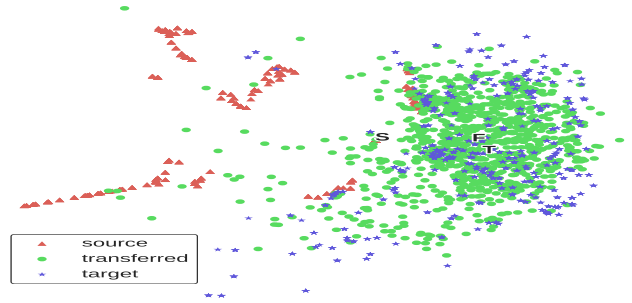


Figure S4. Isomap result.

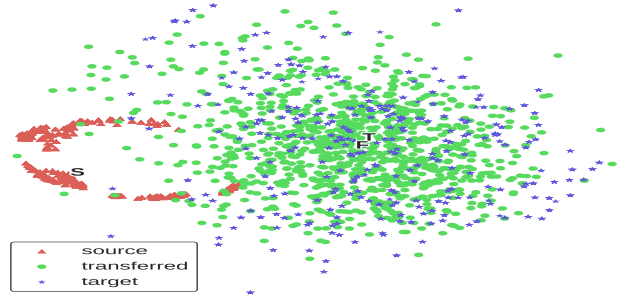


Figure S5. Standard PCA result.

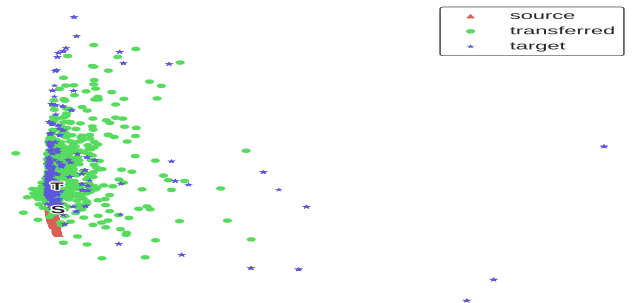


Figure S6. Polynomial kernel PCA result.

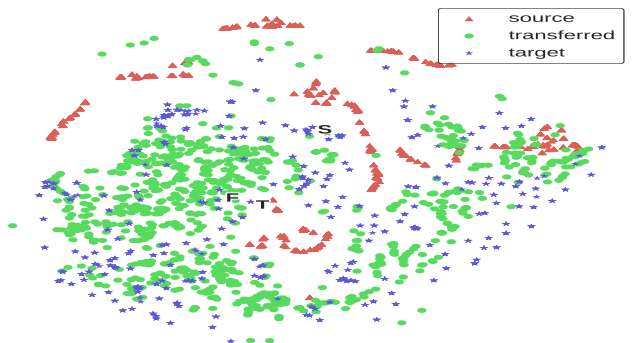


Figure S7. t-SNE result with 1000 images for each domain.